Nano Research
DOI 10.1007/s12274-016-1241-4
Research Article
ISSN 1998-0124
CN 11-5974/O4

Effect of contact- and sliding-mode electrification on nanoscale charge transfer for energy harvesting

Yu Sheng Zhou[1,§], Shengming Li[1,2,§], Simiao Niu[1,§], and Zhong Lin Wang[1,3] (✉)

[1] *School of Materials Science and Engineering, Georgia Institute of Technology, Atlanta, GA 30332 , USA*
[2] *Department of Mechanical Engineering, Tsinghua University, Beijing 100084, China*
[3] *Beijing Institute of Nanoenergy and Nanosystems, Chinese Academy of Sciences, Beijing 100083, China*
[§] *These authors contributed equally to this work.*

Received: 14 June 2016
Revised: 25 July 2016
Accepted: 26 July 2016

KEYWORDS

energy harvesting, contact electrification, triboelectrification, charge transfer, electronic excitation, scanning Kelvin probe microscopy

ABSTRACT

The process of charge transfer based on triboelectrification (TE) and contact electrification (CE) has been recently utilized as the basis for a new and promising energy harvesting technology, i.e., triboelectric nanogenerators, as well as self-powered sensors and systems. The electrostatic charge transfer between two surfaces can occur in both the TE and the CE modes depending on the involvement of relative sliding friction. Does the sliding behavior in TE induce any fundamental difference in the charge transfer from the CE? Few studies are available on this comparison because of the challenges in ruling out the effect of the contact area using traditional macro-scale characterization methods. This paper provides the first study on the fundamental differences in CE and TE at the nanoscale based on scanning probe microscopic methods. A quantitative comparison of the two processes at equivalent contact time and force is provided, and the results suggest that the charge transfer from TE is much faster than that from CE, but the saturation value of the transferred charge density is the same. The measured frictional energy dissipation of ~11 eV when the tip scans over distance of 1 Å sheds light on a potential mechanism: The friction may facilitate the charge transfer process via electronic excitation. These results provide fundamental guidance for the selection of materials and device structures to enable the TE or the CE in different applications; the CE mode is favorable for frequent moderate contact such as vibration energy harvesting and the TE mode is favorable for instant movement such as harvesting of energy from human walking.

1 Introduction

The charge transfer that occurs between two dissimilar surfaces during contact has been a well-known phenomenon for centuries. Two terminologies, namely, triboelectrification (TE) and contact electrification

Address correspondence to zhong.wang@mse.gatech.edu

(CE) have been used to describe this phenomenon based on the involvement of relative sliding friction [1–4]. Both these effects have been recently utilized as the basis for a new and promising energy harvesting technology—triboelectric nanogenerators—as well as for self-powered sensors and systems [5–9]. The selections of material, surface structure and device design for achieving high performance and better stability for this technology as well as other applications directly depend on the friction involved in this phenomenon. However, the fundamental influence of the friction on the charge transfer process is still not clear as there are very few studies in this area. It has been reported that more charges are transferred during the TE than the CE, which is mainly because the actual contact area in TE is much larger than that in CE for any non-ideal flat surface [10–12]. However, the macro-scale characterization method is intrinsically unable to avoid the effect of the change in the contact area during the TE process, making it fairly challenging to probe the fundamental differences between the mechanisms of TE and CE. Therefore, the major obstacle for a more reliable and in-depth study is the lack of a microscopic manipulation and measurement method that can control the micro-contact area and make a fair comparison between the two effects.

The scanning probe microscopic method, notable for its nanometer resolution and controllable contact force, speed, and area, has been recently incorporated for triggering and characterizing the TE process at the nanoscale [13, 14]. It provides a tool for quantitative characterization of the charge transfer. In the present work, we used different working modes of the atomic force microscope (AFM) to trigger the charge transfer between the probe and the sample material, which imitate the two modes of the charge transfer described previously. First, a nanoscale method was introduced based on the tapping mode of AFM to quantitatively characterize CE. Then, for the first time, a fair comparison between CE and TE was realized at the equivalent contact time and the approximate average interaction force. The average contact time and the contact force in TE were quantified through modeling of the cantilever vibration with two tip-sample interactive force regimes. Our results reveal that, given enough contact time, both CE and TE eventually saturate at the same surface charge density, but the charge transfer rate for TE is much faster. According to the measured energy dissipation created by the friction in TE, which is about 11 eV within 1 Å, it is likely that the friction facilitates the charge transfer process during TE via electronic excitation. These results provide fundamental guidance for the selection of the material and the device structure to enable TE or CE in different applications; the CE mode is favorable for frequent moderate contact such as vibration energy harvesting and the TE mode is favorable for instant movements such as harvesting of energy from human walking.

2 Tapping mode AFM as a new method to characterize contact electrification at the nanoscale

Figures 1(a) and 1(b) illustrate the AFM based methods that are used to study CE and TE, respectively. When the AFM is working in the contact (frictional) mode, the AFM tip engages with a constant force against the sample and scans the surface of the sample, which triggers friction-involved TE between the tip and sample surface. On the other hand, in the tapping-mode, the AFM probe vibrates at a certain high frequency and thus interacts with the surface of the sample intermittently in contact-separation cycles, which can simulate the non-frictional CE between the tip and the sample surface. In order to characterize the transferred charge density during the process, we used the abovementioned modes to scan an area in the scale of microns, and then utilized scanning Kelvin probe microcopy (SKPM) for *in situ* measurement of the surface potential change of the rubbed/tapped area. A thin layer of dielectric material with backside grounded is sufficient to correlate the change in the surface potential to the transferred surface charge density using the parallel capacitive model. In the tapping mode, selecting the AFM probe with a certain high resonant frequency and setting a proper scanning speed ensures that the tip has sufficient contact with the sample during the scan, as illustrated in Figs. 1(c) and 1(d). For example, with resonant frequency of 70 kHz and scan speed of 8 μm/s (highest speed in our CE experiments), the tip taps the sample surface

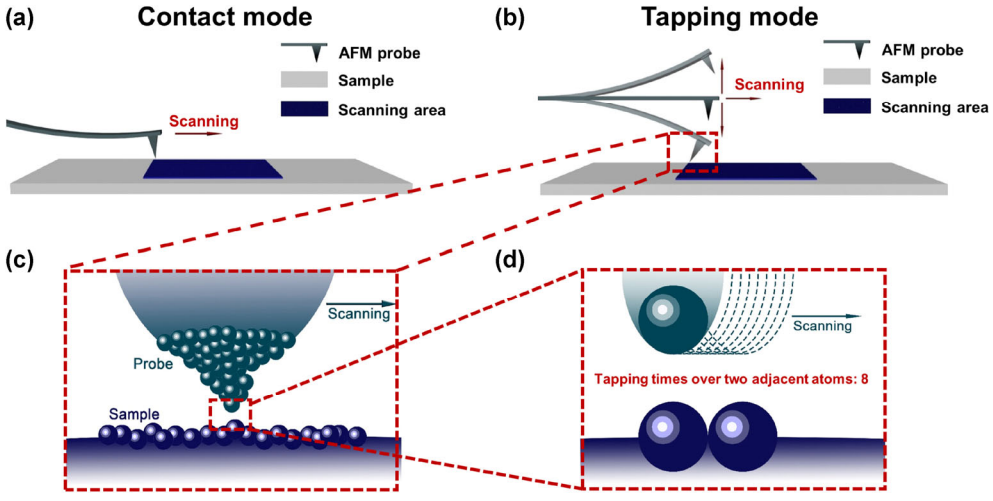

Figure 1 Schematic of the AFM-based methods for TE and CE. (a) TE between the tip and the sample triggered during contact mode AFM. (b) CE triggered during tapping mode AFM. (c) Illustration of the atomic details in the tip-sample contact region. (d) The number of contact cycles in the tapping mode when the tip scans two adjacent atoms, illustrating that the contact is sufficient.

for 87 cycles within a distance equal to the tip radius (~10 nm), and no less than one contact cycle within 1 Å distance. In this way, we ruled out a big issue faced by the researchers while using the traditional methods for studying CE: the coupling of micro-friction caused by the surface roughness.

Since the AFM-based characterization method for studying the TE has been reported in our previous study, here, we introduce the method developed to study the CE using tapping-mode AFM. The probe vibrates at a high frequency (~70 kHz in our experiments) while scanning the sample, making intermittent contact with the surface of the sample. Considering the contact time per cycle (usually less than 10% of the period of a cycle) and the scanning speed (around 0.1–10 μm/s), the lateral displacement during the tap contacts is extremely small (<0.1 Å), ensuring the CE process without the involvement of sliding friction [15].

A sample of parylene thin film was used as an example in the preset study. The AFM was operated in the tapping mode at different values of free amplitudes (A_f) of 50, 70, and 100 nm. The scanning amplitudes (A_s) were set to 60% of A_f on a region of area 4 μm × 4 μm of the sample followed by the surface potential measurement with SKPM on a larger region (~ 16 μm × 16 μm in area). Comparing the surface potentials of the tapped and the surrounding regions, the charge transfer from CE was quantitatively characterized (Fig. 2(a)). For the scan with A_f = 50 nm, there was no distinction in the surface potential from the tapped and the surrounding regions, proving that there is no CE for the tapping scan with these scanning parameters. When we increase A_f to 70 and 100 nm, the surface potential of the tapped regions on the sample dramatically decreased, indicating the occurrence of CE between the tip and the sample. Furthermore, we have also investigated the changes in the phase shift ($\Delta\varphi$) and the vibration amplitude (A) during the approach of the vibrating probe onto the surface of the sample. The relationships, $A - z_c$ and $\Delta\varphi - z_c$ of the vibrating probe at different values of A_f (where, z_c represents the rest distance of the probe cantilever above the sample during the approach) are demonstrated in Fig. 2(b). During the process, the vibration amplitude of the probe decreases with z_c, which is due to the increased energy dissipation when the probe gets closer to the sample surface. On the other hand, as shown in the curves of $\Delta\varphi - z_c$, the change in the phase shift of the vibration has different trends as the probe approaches at different values of A_f. At A_f = 50 nm, there is monotonous increase of $\Delta\varphi$ with the decrease of z_c and A. However, we can observe a sign switch in the $\Delta\varphi - z_c$ curves at A_f = 70 and 100 nm. These results indicate that the tip has already passed through the attractive region on the sample and has entered the repulsive region at its lowest

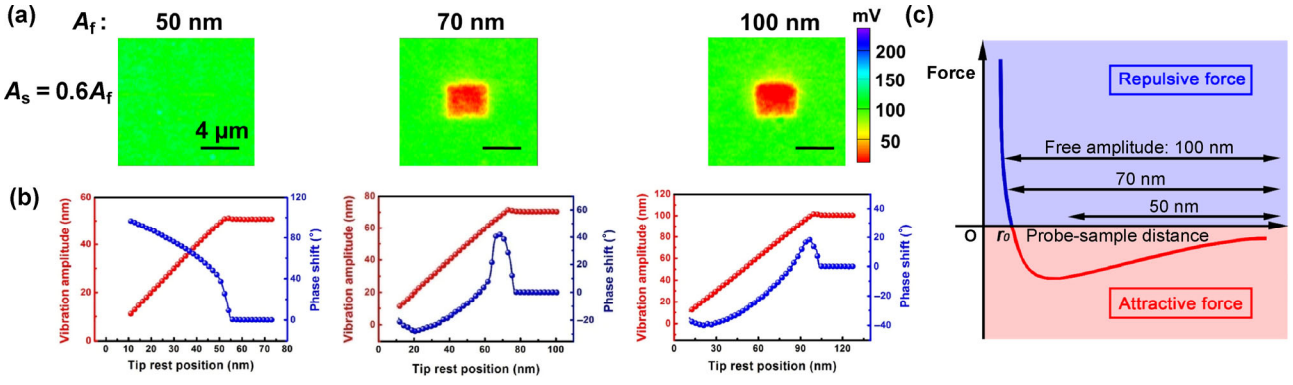

Figure 2 (a) Surface potential mapping on the parylene sample after the AFM tip scanned the central area in the tapping mode at different values of tapping free amplitude. (b) Corresponding AFM probe vibration amplitudes and phase shifts as a function of the tip-sample distance at different tapping amplitudes. (c) Illustration of the tip-sample force curve and the interaction regions at different tapping amplitudes.

position, as the net attractive force on the surface would increase the phase shift ($\Delta\varphi > 0$), while the net repulsive force would decrease the phase shift ($\Delta\varphi < 0$). This change in $\Delta\phi$ with A_f can be understood by the following explanation. The increase in the value of A_f in the tapping process adds more vibration energy to the cantilever, which forces the tip to overcome the attractive force above the sample and enter the repulsive force regime [15–17].

The above experiments indicate that different settings of the tapping scan will result in different CE processes. In order to fully understand this phenomenon, the value of A_f was fixed at 70 nm and the tapping scans were performed at different values of A_s. The resulting surface potential distribution and the curve for ΔV – A_s are shown in Figs. 3(a) and 3(c) (here, ΔV is the difference in the surface potential between the tapped region and the non-contact region demonstrating the effect of CE). There is a dramatic increase in the value of ΔV from 0 to 70 mV at around A_s = 55 nm as A_s decreases. This trend shows the correlation with the vibration phase lag of the AFM probe. As shown in Fig. 3(b), the vibration phase lag, $\Delta\varphi$ increases in the beginning when the value of A_s is comparatively large, while it decreases and stays lower than the free resonating phase lag as the probe approaches closer to the surface (as A_s decreases). The cross-point suggests a switch in the tip-sample interaction force from the attractive to the repulsive regime. This switch corresponds well with the onset point where the surface potential changes, indicating that the CE is predominant when the repulsive force dominates the probe-sample interaction.

Using the above method, the CE process can be simulated and its force and contact time can be controlled by changing the scanning parameters (A_f and A_s) based on the sign of $\Delta\varphi$. This provides the basis for a microscopic and more precise method to study CE.

3 Quantification of contact time and force during contact electrification

In order to compare the CE with the TE quantitatively, we need to know the actual contact time and the force in tapping mode AFM. Driven by an external sinusoidal signal while tapping the surface of the sample, the following model can describe the dynamic motion of the cantilever. This model takes into account, the driving force and the elastic response, the hydrodynamic damping in the medium, as well as the tip-sample interaction and is expressed by a second-order equation as shown below [15, 18, 19]

$$m\frac{\mathrm{d}z^2}{\mathrm{d}^2t} = -k_c z - \frac{m\omega_0}{Q}\frac{\mathrm{d}z}{\mathrm{d}t} + F_{ts} + F_0\cos\omega t \qquad (1)$$

Here, F_0 and ω are the amplitude and the angular frequency of the driving force, respectively and F_{ts} is the dynamic interaction force between the tip and the sample. The symbols, Q, ω_0, and k_c represent the quality factor, the resonant angular frequency, and

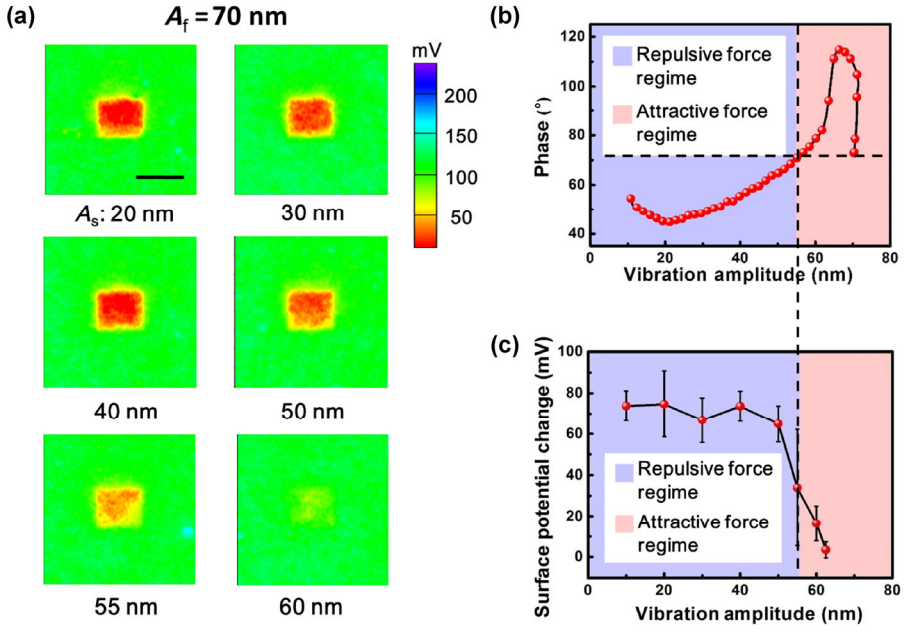

Figure 3 (a) The surface potential mapping of parylene after the AFM tip scanned the central area using different set point amplitudes, with the free vibration amplitude, A_f set to 70 nm. (b) Corresponding phase shift curve as a function of the vibration amplitude of the AFM probe. (c) Plot of the surface potential change as a function of the vibration amplitude.

the spring constant of the free cantilever, respectively. This equation is based on the assumption that the vibrating cantilever with the tip acts like a mass-spring system, and m stands for the effective mass of the cantilever in the equation. In addition, Q as the quality factor of the cantilever is considered to remain constant in the atmosphere. According to the harmonic approximation of the mass-spring model, m and F_0 can be worked out based on the following equations [15, 19]

$$m = \frac{k_c}{\omega_0^2} \tag{2}$$

$$F_0 = A_0 \cdot m \cdot \left[(\omega_0^2 - \omega^2)^2 + \left(\frac{\omega \omega_0}{Q} \right)^2 \right]^{\frac{1}{2}} \tag{3}$$

There are two regions in the interactive force between the tip and the sample: the long-range attractive force region and the short-range repulsive force region. In the attractive force region $(d > a_0)$, the tip and the sample suffer the non-retarded van der Waals forces as illustrated in Fig. 4(a). In the repulsive force region $(d < a_0)$, apart from the van der Waals force which is considered as the adhesion force, there is a repulsive force caused by the Pauli and the ionic repulsions. Therefore, the interactive forces between the tip and the sample (F_{ts}) can be expressed in two parts as shown below [19]

$$F_{ts}(z_c, z) = \begin{cases} -\dfrac{HR}{6(z_c + z)^2} & (d > a_0) \\ \dfrac{4}{3} E^* \sqrt{R} (a_0 - z - z_c)^{3/2} - \dfrac{HR}{6a_0^2} & (d < a_0) \end{cases} \tag{4}$$

Here, H is the Hamaker constant of the interacting material pair (in our experiment, it is platinum coated on the surface of the probe tip, and parylene C as the sample), R is the tip radius, and z_c and d are the rest and the instantaneous separations between the tip and the sample, respectively. In addition, z (with the sign) is the relative distance between the instantaneous and the rest positions of the tip and a_0 is the intermolecular distance. The symbol, E^* represents the effective elastic modulus of the tip-sample system and is calculated according to Eq. (5)

$$\frac{1}{E^*} = \frac{(1 - v_t^2)}{E_t} + \frac{(1 - v_s^2)}{E_s} \tag{5}$$

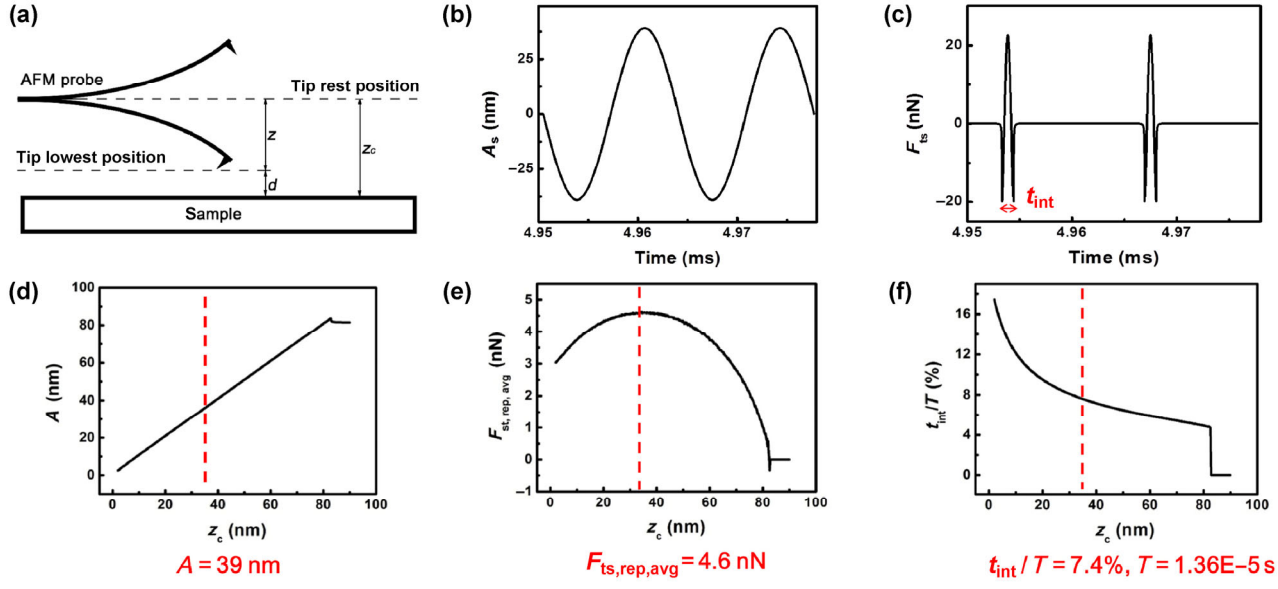

Figure 4 Calculation of the average interaction force between the tip and the sample and the duration for each tapping cycle. (a) Illustration of the positions of the tip-sample interaction. (b) Simulated probe vibration curve. (c) Tip-sample interaction forces in the time domain. (d)–(f) Simulated probe vibration amplitude, average interactive force and repulsive interaction time percentage as a function of set point z_c.

where, $E_t(E_s)$ and $v_t(v_s)$ are the values of the elastic modulus and the Poisson coefficient of the tip (sample), respectively. In the present model, a sphere-flat geometry was used to describe the region of the tip-sample interaction, and we utilized the Derjaguin–Muller–Toporov (DMT) contact mechanics theory to model the repulsive force and the deformation on the sample.

According to our experiment, the parameters used in this simulation are: k_c = 1.5 N/m, $\omega_0 = 73.468k \times 2\pi$ rad/s, $\omega = 73.392k \times 2\pi$ rad/s, A_0 = 81 nm, $H = 12.6 \times 10^{-20}$ J, $E_s = 2.8 \times 10^9$ Pa, $E_t = 1.68 \times 10^{11}$ Pa, v_s = 0.4, v_t = 0.39, R = 28 nm and a_0 = 0.165 nm. The equations of the model were solved using a standard fourth-order Runge–Kutta algorithm. The values of z_c and z are set to 90 and 81 nm, respectively at the beginning of the numerical integration ($z_{c,1}$ = 90 nm, $z_1 = A_0$ = 81 nm), with $dz_1/dt = 0$. At each step of the calculation, the following relationships hold: $z_{c,n} = z_{c,n-1} - dz_c$, $z_n = A_{n-1}$, $dz_n/dt = 0$. The value of A_n is obtained from the curve of z–t, and the values of the average force (F_{rep}) and the duration that the probe tip is in the repulsive force region (t_{int}) are determined from the curve of F_{ts} – t at each z_c (shown in Figs. 4(b) and 4(c), here we take the condition of A_s = 39 nm as the example). Using these values, the relationships, $A_s - z$, $F_{rep} - z$, and $\Delta t_{rep} - z$ are demonstrated, as shown in Figs. 4(d)–4(f).

4 Quantitative comparison of contact electrification and tribo-electrification

We conducted a comparison study of the electron transfer speed and saturation value between CE and TE by performing tapping-mode scans and contact-mode scans (Fig. 5). During both the electrification processes, the deformation on the sample changes due to the different interaction forces on the sample, which leads to changes in the area of the interaction region between the tip and the sample. This change in turn affects the amount of charge transfer. To this consideration, it is necessary to rule out the effect of the interaction area for charge transfer while comparing the CE and the TE, which requires the equalization of the average repulsive force ($F_{rep,avg}$) in the tapping-mode and the interaction force (F_{rep}) in the contact-mode AFM scans. According to our calculation based on the above model, when the value of A_s is set to 39 nm with the value of A_f as 81 nm, the value of $F_{rep,avg}$ is 4.6 nN. In the tapping-mode scans, the scan speeds were set to 8, 4, 2, 1, 0.5 and 0.25 μm/s. With

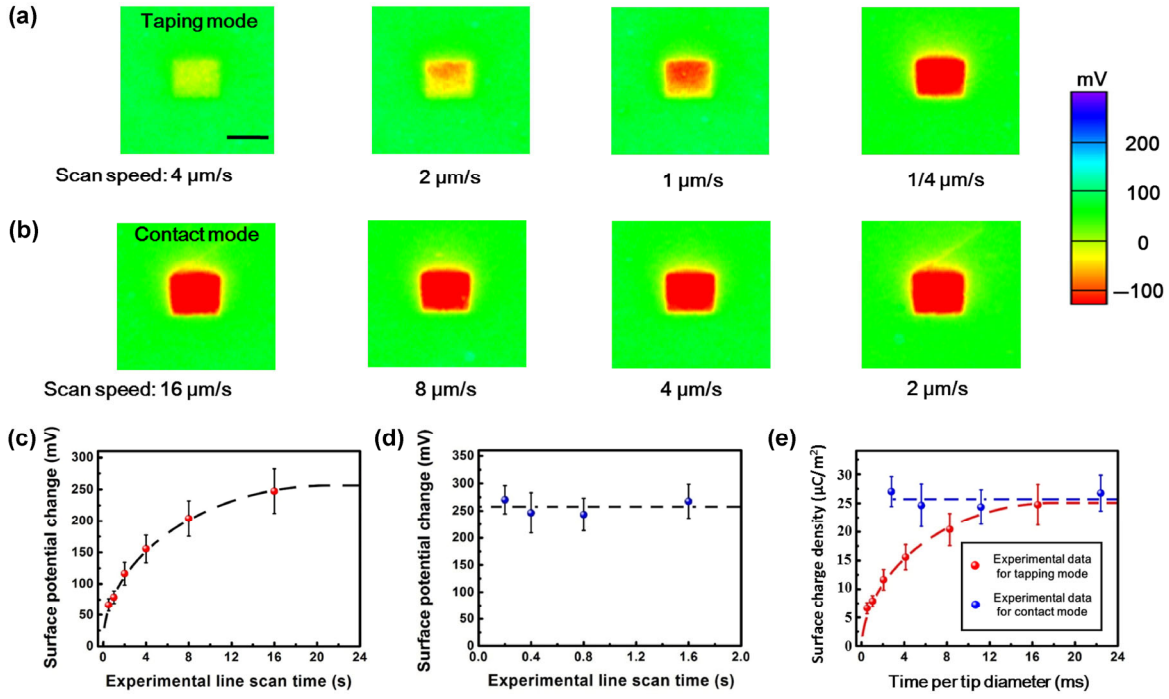

Figure 5 Comparison of charge transfer dynamics between CE and TE. Surface potential mapping of parylene sample after the AFM probe scanned the central area at different scan speeds in (a) the tapping mode and (b) the contact mode. (c) and (d) Corresponding plots of surface potential change as functions of line scan time. (e) Comparison of the charge transfer density triggered by CE and TE as a function of the tip-sample interaction time.

decrease in the scan speed, the surface potential contrast, ΔV increased and saturated to a constant value, as shown in Figs. 5(a) and 5(c). As discussed in Fig. 1, since the sample is tapped 1–29 times with the lateral displacement of only 1 Å using the above scan speeds, there should be negligible change in the contact area compared to the increased contact time among the different conditions of scanning speed. The contact (frictional) mode scans proceeded with a constant force of 4.6 nN and scan speeds of 16, 8, 4 and 2 μm/s. In contrast to the charging results of the CE, the value of ΔV obtained from the frictional mode scan remains constant, indicating that the TE induced charge transfer is not affected by the scan time in this time regime (Figs. 5(b) and 5(d)). In order to make a fair comparison, we need to consider the actual contact time of the CE during the tapping scans, i.e., the time frame when the tip-sample is in the repulsive force regime, because the CE induced charge transfer actually occurs at this condition, as shown in Fig. 2. In our experiment, with A_f = 81 and A_s = 39 nm, the actual contact time is 7.37% of every tapping cycle, as simulated in Fig. 4. Given this conversion, we are able to compare the CE and the TE based on their induced charge density at the equivalent contact time of a tip diameter distance scanning the sample. As shown in Fig. 5(e), the CE induced surface charge density on parylene increased with the contact time and saturated at around 16 ms. In contrast, the surface charge density was steady across the tested time frame for the TE, indicating that the charge density has already saturated even at the highest scan speed in our experiment. Despite the distinction in the electron transfer speed, the charge density in the experiments for both the CE and the TE saturated at the same value.

5 Discussion of the charge transfer mechanism

The differences in the dynamics of charge transfer during the TE process at nanoscale have not been investigated before. It is well known that the friction between two materials leads to dissipation of kinetic energy at the contact interface, in the form of phononic

and/or electronic dissipation mechanisms [20–24]. The latter one usually refers to excitations of the electron–hole pairs [25]. As the charge transfer also occurs at the contact interface, it is likely that the dissipation of the frictional energy is coupled to the charge transfer process, by assisting the electrons to overcome the energy barrier between the two materials. The frictional force in the above contact-mode scanning experiment was measured to be about 17.6 nN, and the associated energy dissipation was calculated to be about 11 eV when the tip scans over distance of 1 Å (in the Electronic Supplementary Material (ESM)). Even though the tip-sample contact has a certain area, only a portion of the atoms in the repulsive force region are activated by the frictional energy to facilitate the charge transfer process owing to the non-flatness at the atomic level. Therefore, from the energy perspective, it is reasonable to attribute the dissipation of the frictional energy to the faster charge transfer dynamics in TE than CE.

6 Conclusion

In summary, this paper provides the first *in-situ* methodology to study CE at the nanoscale based on the combination of tapping mode AFM and SKPM. The charge transfer mainly occurs in the tip-sample repulsive regime in the tapping mode, which was determined by the knowledge of the phase shift in the probe vibration. By calculating the average interaction force and the contact time, we were able to compare the CE with the TE triggered by the contact mode AFM at equivalent contact time and forces. Within the studied contact time regime, the charge transfer from TE is constant during the contact time of 2–20 ms, while that from CE increases when the contact time increases from 2 to 16 ms and saturates at the same magnitude as TE. The energy dissipation at the interfaces of the two contacting materials caused by the friction in TE is measured to be about 11 eV within a distance of 1 Å, which is likely to facilitate the charge transfer process during the TE via electronic excitation. These results provide fundamental guidance for the selection of the material and the device structure to enable TE or CE in different applications; the CE mode is favorable for frequent moderate contact such as vibration energy harvesting and the TE mode is favorable for instant movement such as harvesting of energy from human walking.

Acknowledgements

Research was supported by U.S. Department of Energy, Office of Basic Energy Sciences (No. DE-FG02-07ER46394) and the National Science Foundation (No. DMR-1505319). We also would like to express our sincere appreciation to Dr. Ricardo Garcia for the insightful discussion on modeling and calculation of the dynamic motion of the cantilever in tapping mode AFM.

Electronic Supplementary Material: Supplementary material (additional information and figures, including calibration of lateral deflection sensitivity of the AFM probe used in our system, and measurement of frictional force in triboelectrification process) is available in the online version of this article at http://dx.doi.org/10.1007/s12274-016-1241-4.

References

[1] Horn, R. G.; Smith, D. T. Contact electrification and adhesion between dissimilar materials. *Science* **1992**, *256*, 362–364.

[2] Horn, R. G.; Smith, D. T.; Grabbe, A. Contact electrification induced by monolayer modification of a surface and relation to acid-base interactions. *Nature* **1993**, *366*, 442–443.

[3] Baytekin, H. T.; Patashinski, A. Z.; Branicki, M.; Baytekin, B.; Soh, S.; Grzybowski, B. A. The mosaic of surface charge in contact electrification. *Science* **2011**, *333*, 308–312.

[4] Baytekin, H. T.; Baytekin, B.; Hermans, T. M.; Kowalczyk, B.; Grzybowski, B. A. Control of surface charges by radicals as a principle of antistatic polymers protecting electronic circuitry. *Science* **2013**, *341*, 1368–1371.

[5] Niu, S. M.; Wang, S. H.; Lin, L.; Liu, Y.; Zhou, Y. S.; Hu, Y. F.; Wang, Z. L. Theoretical study of contact-mode triboelectric nanogenerators as an effective power source. *Energy Environ. Sci.* **2013**, *6*, 3576–3583.

[6] Wang, S. H.; Lin, L.; Wang, Z. L. Nanoscale triboelectric-effect-enabled energy conversion for sustainably powering portable electronics. *Nano Lett.* **2012**, *12*, 6339–6346.

[7] Wang, Z. L.; Chen, J.; Lin, L. Progress in triboelectric nanogenerators as a new energy technology and self-powered sensors. *Energy Environ. Sci.* **2015**, *8*, 2250–2282.

[8] Zhou, Y. S.; Zhu, G.; Niu, S. M.; Liu, Y.; Bai, P.; Jing, Q. S.; Wang, Z. L. Nanometer resolution self-powered static and dynamic motion sensor based on micro-grated triboelectrification. *Adv. Mater.* **2014**, *26*, 1719–1724.

[9] Zhu, G.; Zhou, Y. S.; Bai, P.; Meng, X. S.; Jing, Q. S.; Chen, J.; Wang, Z. L. A shape-adaptive thin-film-based approach for 50% high-efficiency energy generation through micro-grating sliding electrification. *Adv. Mater.* **2014**, *26*, 3788–3796.

[10] Ireland, P. M. The role of changing contact in sliding triboelectrification. *J. Phys. D: Appl. Phys.* **2008**, *41*, 025305.

[11] Ohara, K. A method of exponential function analysis of contact and frictional electrification curves. *J. Electrostat.* **1988**, *20*, 319–326.

[12] Tokeshi, T.; Hiratsuka, K.; Sasaki, A.; Uchiyama, S.; Kajdas, C. Triboelectrification in sliding/rolling contacts using twin-ring tribometer. *Tribol. Trans.* **2009**, *52*, 759–767.

[13] Zhou, Y. S.; Liu, Y.; Zhu, G.; Lin, Z. H.; Pan, C. F.; Jing, Q. S.; Wang, Z. L. *In situ* quantitative study of nanoscale triboelectrification and patterning. *Nano Lett.* **2013**, *13*, 2771–2776.

[14] Zhou, Y. S.; Wang, S. H.; Yang, Y.; Zhu, G.; Niu, S. M.; Lin, Z. H.; Liu, Y.; Wang, Z. L. Manipulating nanoscale contact electrification by an applied electric field. *Nano Lett.* **2014**, *14*, 1567–1572.

[15] García, R.; Pérez, R. Dynamic atomic force microscopy methods. *Surf. Sci. Rep.* **2002**, *47*, 197–301.

[16] Cappella, B.; Dietler, G. Force–distance curves by atomic force microscopy. *Surf. Sci. Rep.* **1999**, *34*, 1–104.

[17] Cleveland, J. P.; Anczykowski, B.; Schmid, A. E.; Elings, V. B. Energy dissipation in tapping-mode atomic force microscopy. *Appl. Phys. Lett.* **1998**, *72*, 2613–2615.

[18] García, R.; Gómez, C. J.; Martinez, N. F.; Patil, S.; Dietz, C.; Magerle, R. Identification of nanoscale dissipation processes by dynamic atomic force microscopy. *Phys. Rev. Lett.* **2006**, *97*, 016103.

[19] García, R.; San Paulo, A. Attractive and repulsive tip-sample interaction regimes in tapping-mode atomic force microscopy. *Phys. Rev. B* **1999**, *60*, 4961–4967.

[20] Bhushan, B.; Israelachvili, J. N.; Landman, U. Nanotribology: Friction, wear and lubrication at the atomic scale. *Nature* **1995**, *374*, 607–616.

[21] Braun, O. M.; Naumovets, A. G. Nanotribology: Microscopic mechanisms of friction. *Surf. Sci. Rep.* **2006**, *60*, 79–158.

[22] Marti, O. Nanotribology: Friction on a nanometer scale. *Phys. Scr.* **1993**, *49B*, 599–604.

[23] Singer, I. L. Friction and energy dissipation at the atomic scale: A review. *J. Vac. Sci. Technol. A* **1994**, *12*, 2605–2616.

[24] Krim, J. Friction and energy dissipation mechanisms in adsorbed molecules and molecularly thin films. *Adv. Phys.* **2012**, *61*, 155–323.

[25] Park, J. Y.; Salmeron, M. Fundamental aspects of energy dissipation in friction. *Chem. Rev.* **2014**, *114*, 677–711.